

CCR5 closes the temporal window for memory linking

Yang Shen^{1*}, Miou Zhou^{1,2*}, Denise Cai^{1,3}, Daniel Almeida Filho¹, Giselle Fernandes¹, Ying Cai¹, André F. de Sousa¹, Min Tian⁴, Nury Kim^{5,6}, Jinsu Lee⁶, Deanna Necula¹, Chengbin Zhou¹, Shuoyi Li¹, Shelbi Salinas², Andy Liu¹, Xiaoman Kang¹, Masakazu Kamata⁷, Ayal Lavi¹, Shan Huang¹, Tawnie Silva¹, Won Do Heo⁶, Alcino J. Silva¹

¹Neurobiology, Psychiatry and Psychology Departments & Integrative Center for Learning and Memory, UCLA, Los Angeles, CA.

²Graduate College of Biomedical Sciences, Western University of Health Sciences, Pomona, CA.

³Neuroscience Department, Icahn School of Medicine, 1468 Madison Avenue New York, NY 10029.

⁴Department of Neurology, David Geffen School of Medicine, UCLA, Los Angeles, CA 90095, USA.

⁵Center for Cognition and Sociality, Institute for Basic Science, Daejeon 34126, Republic of Korea.

⁶Department of Biological Sciences, Korea Advanced Institute of Science and Technology,

⁷Department of Hematology and Oncology, UCLA, Los Angeles, CA.

*These authors contributed equally.

Correspondence: silvaa@mednet.ucla.edu, mzhou@westernu.edu

Summary

Real world memories are formed in a particular context and are often not acquired or recalled in isolation¹⁻⁵. Time is a key variable in the organization of memories, since events experienced close in time are more likely to be meaningfully associated, while those experienced with a longer interval are not¹⁻⁴. How does the brain segregate events that are temporally distinct? Here, we report that a delayed (12-24h) increase in the expression of the C-C chemokine receptor type 5 (CCR5), an immune receptor well known as a co-receptor for HIV infection^{6,7}, following the formation of a contextual memory, determines the duration of the temporal window for associating or linking that memory with subsequent memories. This delayed CCR5 expression in mouse dorsal CA1 (dCA1) neurons results in a decrease in neuronal excitability, which in turn negatively regulates neuronal memory allocation, thus reducing the overlap between dCA1 memory ensembles. Lowering this overlap affects the ability of one memory to trigger the recall of the other, thus closing the temporal window for memory linking. Remarkably, our findings also show that an age-related increase in neuronal CCL5/CCR5 expression leads to impairments in memory linking in aged mice, which could be reversed with a CCR5 knockout and an FDA approved drug that inhibits this receptor, a result with significant clinical implications. All together the findings reported here provide the first insights into the molecular and cellular mechanisms that shape the temporal window for memory linking.

Memory formation can be affected by previous experiences. For example, memories acquired close in time often become linked such that the retrieval of one increases the likelihood of retrieving the other (i.e., memory linking). Abnormal memory linking (e.g., improper relational memory), is involved in psychiatric disorders such as post-traumatic stress disorder and schizophrenia^{8,9}. However, very little is known about the mechanisms that regulate interactions amongst memories. Activation of CREB and subsequent increases in neuronal excitability are thought to open the temporal window for memory linking, so that a given neuronal ensemble

47 involved in encoding one memory is more likely to participate in encoding a second memory
48 acquired close in time^{2,10-13}. Accordingly, the neuronal overlap between memory ensembles has
49 been shown to be critical for memory linking¹⁻³. In contrast, little is known about the mechanisms
50 that segregate events that are temporally distinct. CCR5 has been extensively studied in the context
51 of inflammatory responses and HIV infection^{6,7}. However, comparatively little is known about its
52 role in learning and memory. Both CCR5 and its ligand CCL5 are highly enriched in the CA1
53 region of the hippocampus¹⁴⁻¹⁶, and CCR5 is a negative regulator of CREB activation and neuronal
54 excitability^{15,17}. Here, we demonstrate that a gradual increase in the expression of CCL5/CCR5
55 following memory formation closes the temporal window for memory linking, thus segregating
56 memories that are temporally distinct.

57

58 **CCR5 expression is enhanced after learning**

59 To explore CCR5's role in contextual memory linking, where the memory of one context is
60 associated or linked to the memory of a second context¹, we first tested whether the expression of
61 CCR5 and its ligands changes after contextual conditioning (Fig. 1a) in a brain region critical for
62 this form of learning (i.e., dCA1). Compared to expression levels in mice that stayed in their home
63 cage (HC), both *Ccr5* and *Ccl5* mRNA increased 12 hours (12h) after contextual conditioning
64 (Fig. 1b, c), while there were no significant changes in the expression of other CCR5 ligands tested
65 (*Ccl3*, *Ccl4* and *Ccl11*; Extended Data Fig. 1a-d). Next, we used *in situ* hybridization to determine
66 the hippocampal cellular distribution of this learning-induced increase in *Ccr5* expression (Fig.
67 1d). Although in dCA1 of HC mice there were more *Ccr5*-expressing microglia than *Ccr5*-
68 expressing neurons (Fig. 1e), there was a dramatic increase in *Ccr5*-expressing neurons, but not
69 microglia, at 6h and 12h after contextual conditioning (Fig. 1f). Further analysis showed that the
70 increase was mainly in excitatory neurons (Extended Data Fig. 1e, f). Unlike *Ccr5*, in dCA1 of
71 HC mice there were more *Ccl5*-expressing neurons than *Ccl5*-expressing microglia, which is
72 consistent with previous report¹⁴, while no obvious changes in the number of *Ccl5*-expressing
73 neurons or microglia were observed (Extended Data Fig. 1g-i). To examine whether *Ccr5* is
74 primarily expressed in memory ensemble cells after learning, we used either the cFos-tTA
75 transgenic mice and AAV-TRE-mCherry virus to label neurons involved in contextual memory,
76 or the Chr2_{E123T/T159C} (ETTC) to pre-activate a set of neurons before contextual learning to increase
77 the probability that these neurons would be involved in the contextual memory¹⁸. With both
78 methods, we found that *Ccr5* had a significantly higher probability to be expressed in memory
79 ensemble cells than chance (Extended Data Fig. 2).

80 In addition to CCR5 expression, we also measured neuronal CCR5 activity after learning with
81 the *iTango2* approach¹⁹ (Fig. 1g). The light- and ligand-gated gene expression system we
82 constructed (CCR5-*iTango2*) enables cellular expression of a reporter gene (i.e., EGFP) only in
83 the presence of both CCR5 ligand(s) and blue-light exposure (detailed information in Methods).
84 When tested in either HEK293 cells (Extended Data Fig. 3a-j), in dCA1 (Fig. 1h; Extended Data
85 Fig. 4a-c), or in the dentate gyrus (Extended Data Fig. 3k-m), CCR5-*iTango2* showed a significant
86 increase in EGFP expression only when both light and ligand (CCL5) were present, demonstrating
87 that CCR5-*iTango2* is capable of monitoring ligand dependent CCR5 activation. Therefore,
88 CCR5-*iTango2* viruses were injected into mouse dCA1, and 3 weeks later mice were trained with
89 contextual fear conditioning. Compared to HC controls, there was a gradual increase in neuronal

90 CCR5 activity in trained mice after conditioning (Fig. 1i, j), a result consistent with the delayed
91 expression patterns of CCR5 and CCL5 presented above (Fig. 1b, c and f). Notably, CCR5
92 activation measured by CCR5-*i*Tango2 also showed a selectivity for memory ensemble cells after
93 learning (Extended Data Fig. 4g-i).

94 Overall, our results demonstrated that after contextual learning there was a delayed (12-24h)
95 increase in CCL5/CCR5 signaling in dCA1 neurons, especially in the neurons involved in
96 contextual learning.

97

98 **CCR5 regulates contextual memory linking**

99 To determine whether CCR5 modulates the temporal window for contextual memory linking¹, we
100 first exposed the mice to one context (context A) and either 5h, 1, 2 or 7 days later we exposed the
101 mice to a second context (context B) (Fig. 2a). Two days later, the mice were given an immediate
102 shock in context B, and then contextual memory linking was tested 2d later in context A. During
103 the memory linking test, the 5h group showed higher freezing (i.e., higher linking) than the 1d, 2d
104 or the 7d groups. This result shows that contextual memory linking decreases significantly between
105 5h and 1d, indicating a time course parallel to the increase in CCR5 signaling after learning (Fig.
106 1). Therefore, we subsequently investigated whether increasing or inhibiting CCR5 signaling
107 affected the temporal window for contextual memory linking.

108 We first enhanced CCR5 activity by infusing CCL5 into dCA1 4h after mice were exposed to
109 context A, a time point that preceded the expected endogenous CCR5 signaling increase. During
110 the contextual memory linking test, compared to the control group, the CCL5 group showed
111 significantly lower freezing in context A than the mice had explored 5h before context B (Fig. 2b),
112 indicating that increasing CCR5 activity led to an attenuation of contextual memory linking.
113 Notably, mice in both the control and CCL5 groups had higher freezing in the 5h context than in
114 a novel context, suggesting that besides the CCL5/CCR5 signaling pathway, other mechanisms,
115 including those involving other CREB inhibitors or inhibitory microcircuits² might also regulate
116 the temporal window for memory linking. We then tested whether contextual memory linking could
117 be regulated specifically by direct manipulation of neuronal CCR5 activity with a genetically
118 encoded optical tool (Opto-CCR5) with high spatiotemporal precision²⁰ (Fig. 2c; detailed
119 information in Methods). Consistent with CCR5 activation²¹⁻²⁴, light stimulation of Opto-CCR5
120 caused both a significant enhancement of intracellular Ca²⁺ and phosphorylation of Erk1/2
121 (Extended Data Fig. 5a-e). To ensure specific neuronal expression, AAV1-hSyn-Cre was co-
122 injected with Lenti-EF1a-DIO-Opto-CCR5 (or EGFP control virus) into dCA1 (Fig. 2d and
123 Extended Data Fig. 5f). During the contextual memory linking test, only the control group, but not
124 the Opto-CCR5 group, showed evidence of memory linking (i.e., higher freezing in context A, that
125 the mice experienced 5h before context B, compared to a novel context; Fig. 2e), confirming that
126 increasing neuronal CCR5 activity specifically after exposure to context A is sufficient to impair
127 contextual memory linking without impairing memory for context B.

128 To examine whether attenuating CCR5 signaling could extend the window for contextual
129 memory linking, AAV8 containing shRNA-Control or shRNA-CCR5 was injected into dCA1
130 (Fig. 2f). Three weeks later, mice were pre-exposed to context A and then context B with a 2d
131 interval. As expected, during testing, the control group did not show memory linking (i.e., showed
132 similar freezing in context A as in a novel context; Fig. 2f). In contrast, the shRNA-CCR5 group

133 showed higher freezing in context A than in a novel context, and there was no difference in freezing
134 between contexts A and B, demonstrating strong memory linking (Fig. 2f).

135 Additionally, *Ccr5* knockout mice (*Ccr5*^{-/-} mice) were also tested for contextual memory
136 linking. As expected, during the test in context A, the WT mice froze less when the interval
137 between contexts was 7d versus 5h. In contrast, *Ccr5*^{-/-} mice showed similar freezing in context A
138 when the intervals between context A and B were 5h or 7d. These freezing levels were also similar
139 to those shown in the shocked context (context B; Fig. 2g), demonstrating strong memory linking
140 in *Ccr5*^{-/-} mice with a time interval (i.e., 7d) when WT mice do not show memory linking. Thus,
141 two very different manipulations that decreased the levels of CCR5 (shRNA-mediated knockdown
142 and a knockout) extended the temporal window for memory linking. Similar to *Ccr5*^{-/-} mice, *Ccl5*
143 knockout (*Ccl5*^{-/-}) mice also showed an extended linking window (Extended Data Fig. 6g),
144 indicating that CCL5 is critical for CCR5 regulation of memory linking. To test whether CCR5
145 regulates linking for other forms of memory, we developed a memory linking task based on place
146 preference with saccharin water used as a reward (Extended Data Fig. 6a). As with contextual
147 memory linking with fear conditioning, the mice were able to link two memories when they were
148 separated by 5h but not 7d (Extended Data Fig. 6b-d). Additionally, CCL5 infusion to dCA1 also
149 inhibited memory linking in this appetitive linking task tested with a 5h interval, demonstrating
150 that CCR5 activation inhibits both forms of memory linking (Extended Data Fig. 6e, f).

151 Altogether, our results show that increasing or inhibiting CCR5 signaling impaired or extended
152 (respectively) the temporal window for contextual memory linking, demonstrating a key role for
153 CCR5 in setting the duration for the memory linking window.

154

155 **CCR5 modulates memory co-allocation**

156 Next, we investigated how CCR5 regulates the temporal window for contextual memory linking.
157 Previous results suggested that a temporary increase in neuronal excitability following learning^{25,26}
158 biases the allocation of a subsequent memory to the neuronal ensemble encoding the initial
159 memory¹, and that this ensemble overlap was critical for memory linking²⁷. Thus, we examined
160 whether CCR5 modulated neuronal excitability and consequently memory ensemble overlap, since
161 this could explain CCR5's role in shaping the temporal window for memory linking. When treated
162 with CCL5, dCA1 neurons from acute hippocampal slices showed a decrease in current injection-
163 induced firing rate (Fig. 3a, b), indicating an inhibition of neuronal excitability. This is a significant
164 result, since neuronal excitability is critical for determining which specific neurons in a neural
165 network will store a given memory (known as memory allocation)^{13,18,28}. Importantly, decreases
166 in excitability, caused by increases in CCR5 signaling following learning, could explain how this
167 receptor decreases memory ensemble overlap, and thus closes the window for memory linking.

168 To directly test whether increases in CCR5 activity could decrease memory allocation, Opto-
169 CCR5-EGFP or the EGFP control were expressed in mouse dCA1, and then subjected to blue light
170 for 30 min (at different light power levels) before context exploration (Fig. 3c). Following light
171 activation (4 and 8 mW) and contextual training, dCA1 neurons expressing Opto-CCR5 showed a
172 significant reduction in the expression of learning-induced c-Fos, a widely used marker for neurons
173 involved in memory²⁹ (Fig. 3d, e), while the number of overall c-Fos⁺ or EGFP cells were similar
174 among groups (Extended Data, Fig. 7g, h). This result supports the hypothesis that CCR5
175 activation excludes neurons from memory ensembles. Additionally, light activation did not cause

176 any changes in c-Fos expression in the EGFP⁺ cells in the EGFP control group (Extended Data,
177 Fig. 7e, f). Furthermore, when AAV8 containing shRNA-CCR5 was injected into dCA1, neurons
178 with *Ccr5* knockdown had a higher probability of expressing c-Fos (i.e., being involved in
179 memory; Extended Data, Fig. 7a, b) compared with control neurons, a result that also supports the
180 hypothesis that CCR5 activity modulates memory allocation in neuronal networks.

181 Altogether, the results presented suggest that the increase in CCR5 expression and signaling
182 after learning prevents subsequent memories from being allocated to the neuronal ensemble
183 encoding the initial memory, thus reducing the overlap between the two memory ensembles, and
184 consequently attenuating memory linking. To test this hypothesis, we first labeled the memory
185 neural ensembles activated by two contextual exposures with the cFos-tTA/TRE-mCherry system
186 and with *c-Fos* mRNA *in situ* hybridization. There was significantly higher *Ccr5* expression in the
187 non-overlapping neuronal ensemble population than in the overlapping population, and there was
188 a negative correlation between *Ccr5* expression in cells encoding the first contextual memory and
189 the probability of overlap between the two memory ensembles (Fig. 3f-h), indicating that increased
190 *Ccr5* expression in the first memory engram reduces the overlap between the two memory
191 ensembles.

192 To further test this hypothesis, we recorded neuronal calcium activity (with GCaMP6f) in dCA1
193 with head mounted fluorescent microscopes (miniscopes¹) while mice were exploring two
194 different contexts separated by either 5h, 1d, 2d, or 7d. Then, we measured the overlap between
195 the active neuronal populations recorded during the two contextual exposures in both WT and
196 *Ccr5* knockout mice (Fig. 3i, j). Compared to WT mice, *Ccr5*^{-/-} mice revealed an overall
197 significantly higher neural ensemble overlap (Fig. 3k). Neurons in a contextual memory ensemble
198 were reported to have significantly higher mean firing rate³⁰. Therefore, we next focused our
199 analyses on the cells with high (top 10%) activity during the contextual exposures. There was a
200 time dependent reduction in neuronal activity of this group of cells with high activity in WT mice,
201 while no reduction was observed in *Ccr5*^{-/-} mice (Extended Data Fig. 8). When the overlap between
202 high activity cells was measured, a time-dependent (5h vs 2d) decrease in overlap was observed
203 in WT mice, and this decrease was attenuated by the *Ccr5* KO (Extended Data Fig. 9). Altogether
204 these results support the hypothesis that CCR5 modulates the temporal window for memory
205 linking by regulating neuronal co-allocation and consequently the overlap between memory
206 ensembles.

207

208 **CCR5 and aging-related linking deficits**

209 CCR5 and CCL5 expression in peripheral immune cells increases with age^{31,32}. Similar increases
210 in aging neurons could contribute to age-related decreases in contextual memory linking¹. To test
211 this hypothesis, we measured hippocampal *Ccr5* and *Ccl5* expression in 16~18-month-old mice
212 (middle-aged), an age in which mice still show intact contextual conditioning, but deficits in
213 contextual memory linking¹. Compared with young mice, middle-aged home cage mice had
214 significantly enhanced *Ccl5* and *Ccr5* mRNA levels (Fig. 4a). Middle-aged mice also showed an
215 increase in the transient *Ccl5* expression at 3h following contextual learning (Fig. 4b), which was
216 earlier than in young mice (6-12h after learning, Fig. 1c). *In situ* hybridization showed that the
217 increase in *Ccr5* and *Ccl5* expression was mainly in neurons (Fig. 4c-f).

218 Although middle-aged WT mice showed deficits in contextual memory linking¹, even when
219 short intervals (i.e., 5h) were used (Fig. 4g), middle-aged *Ccr5*^{-/-} mice showed clear evidence for
220 memory linking tested with a 5h interval (i.e., higher freezing in contexts A than in a novel context;
221 Fig. 4g). To test the effect of pharmacologically blocking CCR5 activity on contextual memory
222 linking in middle-aged mice, maraviroc (an FDA approved CCR5 antagonist used for HIV
223 treatment; Extended Data Fig. 4d-f)³³ was infused to dCA1 of these mice 1h before they were
224 exposed to context B in a contextual memory linking experiment with a 5h interval. Unlike control
225 mice, maraviroc-treated mice showed memory linking (Fig. 4h). Thus, blocking CCR5 with
226 maraviroc ameliorates the memory linking deficits in middle-aged mice. Altogether these results
227 support a role for CCR5 expression in closing the temporal window for memory linking as well as
228 in age-related deficits in memory linking.

229 In summary, the findings reported here show that a delayed (12-24h) increase in CCL5/CCR5
230 signaling in dCA1 neurons of a given memory ensemble closes the temporal window for memory
231 linking. CCR5 activation decreases neuronal excitability, thus negatively regulating memory
232 allocation. This change in memory allocation decreases the overlap between memory ensembles,
233 and therefore impairs the ability of one memory to trigger the recall of the other, thus closing the
234 temporal window for memory linking (Extended Data Fig. 10). Remarkably, our findings also
235 show that an age-related increase in CCL5/CCR5 expression leads to impairments in memory
236 linking in middle-aged mice that could be reversed with an FDA approved drug that inhibits this
237 receptor, a result with significant clinical implications. All together the findings reported here
238 provide the first insights into the molecular and cellular mechanisms that close the temporal
239 window for memory linking, thus segregating the memories for events that are temporally distinct.
240

241 **Figure legend**

242
243 **Fig. 1| CCR5 expression and activation in the dorsal hippocampus after contextual fear**
244 **conditioning.**

245 **a-c**, mRNA levels of *Ccr5* (**b**) and *Ccl5* (**c**) in mouse dCA1 at 3-24h after fear conditioning (**a**).
246 Tissue (dCA1) from home cage (HC) mice was collected at the same time points (3-24h) and
247 pooled together as the control HC group. Results were normalized to HC (*Ccr5*: HC n=18, 3 h
248 n=7, 6 h n=8, 12 h n=8, 24 h n=10 mice; *Ccl5*: HC n=11, 3 h n=4, 6 h n=8, 12 h n=8, 24 h n=8
249 mice; **P* < 0.05, one-way ANOVA).

250 **d**, Representative images of *Ccr5*, *Itgam* (microglial marker), and *Rbfox3* (neuronal marker)
251 mRNA expression in dCA1 from naïve mice or mice 3-24h after fear conditioning. Red arrows:
252 cells expressing *Ccr5* and *Itgam*. Orange arrows: cells expressing *Ccr5* and *Rbfox3*. Scale bar, 20
253 μ m.

254 **e**, Number of *Ccr5*-expressing microglia and neurons in naïve mice (n=5 mice per group; **P* <
255 0.05, paired t-test).

256 **f**, Number of *Ccr5*-expressing microglia and neurons 3-24h after fear conditioning (HC n=5, 3 h
257 n=4, 6 h n=5, 12 h n=4, 24 h n=4 mice; **P* < 0.05, ***P* < 0.01, two-way repeated measures
258 ANOVA).

259 **g**, Schematics for CCR5-*i*Tango2.

260 **h**, Representative images of CCR5-*i*Tango2-expressing dCA1 neurons after treatment with CCL5,
261 DAPTA (CCR5 antagonist) and light stimulation. Scale bar, 50 μ m.

262 **i**, Representative images of CCR5-*i*Tango2-expressing dCA1 neurons after fear conditioning.
263 Scale bar, 50 μ m.
264 **j**, Quantification of EGFP expression (intensity normalized to tdTomato which is tagged to β -
265 Arrestin through P2A, reflecting expression of the *i*Tango system. HC n=5, 3 h n=6, 6 h n=6, 12
266 h n=5, 24 h n=5 mice; * P < 0.05, one-way ANOVA).
267 All results shown as mean \pm s.e.m.

268

269 **Fig. 2| CCR5 regulates the temporal window of memory linking.**

270 **a**, Characterization of the temporal window for contextual memory linking (Ctx A, Context A; Ctx
271 B, Context B; 5h n=32, 1d n=26, 2d n=14, 7d n=16 mice; * P < 0.05, one-way ANOVA).

272 **b**, CCL5 infusion in dCA1 attenuated 5h contextual memory linking (Veh n=20, CCL5 n=17 mice;
273 * P < 0.05, **** P < 0.0001, two-way repeated measures ANOVA).

274 **c**, Schematics of the Opto-CCR5 construct.

275 **d**, Schematics of viral constructs injection. Scale bar, 500 μ m.

276 **e**, Optogenetic activation of neuronal CCR5 impaired 5h contextual memory linking (Control
277 n=15, Opto-CCR5 n=14 mice; * P < 0.05, *** P < 0.001, two-way repeated measures ANOVA).

278 **f**, Left: Schematics of AAV8-shCon or AAV8-shCCR5 intrahippocampal injection. Scale bar, 500
279 μ m. Right: *Ccr5* knockdown in dCA1 neurons extended the temporal window of contextual
280 memory linking (shRNA-Cont n=14, shRNA-CCR5 n=16 mice; * P < 0.05, ** P < 0.01, two-way
281 repeated measures ANOVA).

282 **g**, *Ccr5* knockout extended the temporal window of contextual memory linking (WT n=9, *Ccr5*^{+/-}
283 n=6, *Ccr5*^{-/-} n=7 mice; * P < 0.05, ** P < 0.01, two-way repeated measures ANOVA).

284 All results shown as mean \pm s.e.m.

285

286 **Fig. 3| CCR5/CCL5 modulate neuronal excitability, memory allocation and the overlap of**
287 **memory ensembles.**

288 **a**, Schematics of neuronal recordings and representative traces.

289 **b**, dCA1 neurons treated with CCL5 for 1h showed a significant decrease in firing rate (Control
290 n=10 cells, CCL5 n=9 cells, * P < 0.05, two-way repeated measures ANOVA).

291 **c**, Representative images of colocalization between c-Fos and Opto-CCR5-EGFP after light
292 stimulation and novel context exposure. Scale bar, 50 μ m.

293 **d**, Percentage of c-Fos⁺EGFP⁺ cells at different power levels (0 mW n=13, 2 mW n=3, 4 mW n=5,
294 8 mW n=3 mice; *** P < 0.001, two-way repeated measures ANOVA).

295 **e**, Colocalization between c-Fos⁺ cells and EGFP⁺ cells after normalization to chance level. (0 mW
296 n=13, 2 mW n=3, 4 mW n=5, 8 mW n=3 mice; * P < 0.05, ** P < 0.01, one-way ANOVA).

297 **f**, Schematics & representative images of *Ccr5* expression and the overlap between memory
298 ensembles of context A (*mCherry*) and context B (*c-Fos*) with a 12h interval between the two
299 contextual exposures. Scale bar, 20 μ m.

300 **g**, The probability of *Ccr5* expression in the overlapping cells is lower than that in the non-
301 overlapping cells (n=6 mice; ** P < 0.01, paired t-test).

302 **h**, Probability of ensemble overlap (between context A and context B) and *Ccr5* expression in
303 *mCherry*⁺ cells (ensemble for context A) are negatively correlated (n=6 mice; $R^2=0.7081$, P < 0.05).

304 **i**, Schematics for miniscope setup and calcium signal identification. Images were collected from
305 mice exploring different contexts separated by either 5h, 1d, 2d, or 7d. Scale bar, 50 μ m.

306 **j**, Neuronal overlap between different contexts. Scale bar, 50 μ m.

307 **k**, Overlapping index for WT and *Ccr5*^{-/-} mice (WT n=6, and *Ccr5*^{-/-} n=6 mice; ***P* < 0.01, two-
308 way ANOVA).

309 All results shown as mean ± s.e.m.

310

311 **Fig. 4| Enhanced CCL5/CCR5 signaling contributes to age-related memory linking deficits.**

312 **a**, Middle-aged HC mice had higher *Ccr5* and *Ccl5* mRNA levels in dCA1 than young HC mice
313 (*Ccr5*: young n=14, aged n=6, *Ccl5*: young n=12, aged n=5; **P* < 0.05, *****P* < 0.0001, Student's
314 t-test).

315 **b**, *Ccr5* and *Ccl5* expression after fear conditioning in dCA1 of middle-aged mice (*Ccr5*: n=6 for
316 all groups, *Ccl5*: HC n=5, 3h n=6, 6h n=6; ***P* < 0.01, ****P* < 0.001, one-way ANOVA).

317 **c**, Representative images of *Ccr5*, *Itgam* and *Rbfox3* mRNA expression in dCA1 from naïve young
318 or middle-aged mice. Red arrows: cells expressing *Ccr5* and *Itgam*. Orange arrows: cells
319 expressing *Ccr5* and *Rbfox3*. Scale bar, 50 µm.

320 **d**, Number of *Ccr5*-expressing microglia and neurons in young or middle-aged mice (young n=5,
321 aged n=4 mice; **P* < 0.05, Student's t-test).

322 **e**, Representative images of *Ccl5*, *Itgam* and *Rbfox3* mRNA expression in dCA1 from naïve young
323 or middle-aged mice. Red arrows: cells expressing *Ccr5* and *Itgam*. Orange arrows: cells
324 expressing *Ccr5* and *Rbfox3*. Scale bar, 50 µm.

325 **f**, Number of *Ccl5*-expressing microglia and neurons in young or middle-aged mice (n=5 mice;
326 ****P* < 0.001, Student's t-test).

327 **g**, *Ccr5* knockout rescued 5h memory linking deficits in middle-aged mice (WT n=7, *Ccr5*^{-/-} n=8;
328 ***P* < 0.01, ****P* < 0.001, two-way repeated measures ANOVA).

329 **h**, Maraviroc, a CCR5 antagonist, rescued 5h memory linking deficits in middle-aged mice (Veh
330 n=15, maraviroc n=14; **P* < 0.05, ***P* < 0.01, two-way repeated measures ANOVA).

331 All results shown as mean ± s.e.m.

332

333 **Data availability**

334 The original videos and datasets generated during and/or analyzed during the current study are
335 available from the corresponding authors.

336

337 **Code availability**

338 Analysis codes are freely available at <https://github.com/Almeida-FilhoDG/ConcatMiniscope>.

339

340 **References**

- 341 1 Cai, D. J. *et al.* A shared neural ensemble links distinct contextual memories encoded close in
342 time. *Nature* **534**, 115-118 (2016).
- 343 2 Rashid, A. J. *et al.* Competition between engrams influences fear memory formation and recall.
344 *Science* **353**, 383-387 (2016).
- 345 3 Abdou, K. *et al.* Synapse-specific representation of the identity of overlapping memory engrams.
346 *Science* **360**, 1227-1231, doi:10.1126/science.aat3810 (2018).
- 347 4 Yetton, B. D., Cai, D. J., Spoormaker, V. I., Silva, A. J. & Mednick, S. C. Human Memories Can Be
348 Linked by Temporal Proximity. *Front Hum Neurosci* **13**, 315, doi:10.3389/fnhum.2019.00315
349 (2019).
- 350 5 Mack, M. L., Love, B. C. & Preston, A. R. Building concepts one episode at a time: The
351 hippocampus and concept formation. *Neurosci Lett* **680**, 31-38,
352 doi:10.1016/j.neulet.2017.07.061 (2018).

353 6 Zhou, L. & Saksena, N. K. HIV Associated Neurocognitive Disorders. *Infect.Dis.Rep.* **5**, e8 (2013).
354 7 Ellis, R., Langford, D. & Masliah, E. HIV and antiretroviral therapy in the brain: neuronal injury
355 and repair. *Nat Rev Neurosci* **8**, 33-44, doi:10.1038/nrn2040 (2007).
356 8 Jung, W. & Lee, S. H. Memory deficit in patients with schizophrenia and posttraumatic stress
357 disorder: relational vs item-specific memory. *Neuropsychiatr Dis Treat* **12**, 1157-1166,
358 doi:10.2147/ndt.S104384 (2016).
359 9 Avery, S. N. *et al.* Impaired relational memory in the early stage of psychosis. *Schizophr Res* **212**,
360 113-120, doi:10.1016/j.schres.2019.07.060 (2019).
361 10 Czajkowski, R. *et al.* Encoding and storage of spatial information in the retrosplenial cortex.
362 *Proc.Natl.Acad.Sci.U.S.A* **111**, 8661-8666 (2014).
363 11 Han, J. H. *et al.* Selective erasure of a fear memory. *Science* **323**, 1492-1496,
364 doi:10.1126/science.1164139 (2009).
365 12 Sano, Y. *et al.* CREB regulates memory allocation in the insular cortex. *Curr Biol* **24**, 2833-2837,
366 doi:10.1016/j.cub.2014.10.018 (2014).
367 13 Zhou, Y. *et al.* CREB regulates excitability and the allocation of memory to subsets of neurons in
368 the amygdala. *Nat Neurosci* **12**, 1438-1443, doi:10.1038/nn.2405 (2009).
369 14 Lanfranco, M. F., Mocchetti, I., Burns, M. P. & Villapol, S. Glial- and Neuronal-Specific Expression
370 of CCL5 mRNA in the Rat Brain. *Front Neuroanat.* **11**, 137 (2017).
371 15 Zhou, M. *et al.* CCR5 is a suppressor for cortical plasticity and hippocampal learning and
372 memory. *Elife* **5**, doi:10.7554/eLife.20985 (2016).
373 16 Torres-Muñoz, J. E., Van Waveren, C., Keegan, M. G., Bookman, R. J. & Petito, C. K. Gene
374 expression profiles in microdissected neurons from human hippocampal subregions. *Brain Res*
375 *Mol Brain Res* **127**, 105-114, doi:10.1016/j.molbrainres.2004.05.017 (2004).
376 17 Shepherd, A. J., Loo, L. & Mohapatra, D. P. Chemokine co-receptor CCR5/CXCR4-dependent
377 modulation of Kv2.1 channel confers acute neuroprotection to HIV-1 glycoprotein gp120
378 exposure. *PLoS One* **8**, e76698, doi:10.1371/journal.pone.0076698 (2013).
379 18 Yiu, A. P. *et al.* Neurons are recruited to a memory trace based on relative neuronal excitability
380 immediately before training. *Neuron* **83**, 722-735, doi:10.1016/j.neuron.2014.07.017 (2014).
381 19 Lee, D. *et al.* Temporally precise labeling and control of neuromodulatory circuits in the
382 mammalian brain. *Nat Methods* **14**, 495-503, doi:10.1038/nmeth.4234 (2017).
383 20 Airan, R. D., Thompson, K. R., Fenno, L. E., Bernstein, H. & Deisseroth, K. Temporally precise in
384 vivo control of intracellular signalling. *Nature* **458**, 1025-1029, doi:10.1038/nature07926 (2009).
385 21 Shideman, C. R., Hu, S., Peterson, P. K. & Thayer, S. A. CCL5 evokes calcium signals in microglia
386 through a kinase-, phosphoinositide-, and nucleotide-dependent mechanism. *J Neurosci Res* **83**,
387 1471-1484, doi:10.1002/jnr.20839 (2006).
388 22 Marozsan, A. J. *et al.* Mechanisms involved in stimulation of human immunodeficiency virus type
389 1 replication by aminooxypentane RANTES. *J Virol* **75**, 8624-8638, doi:10.1128/jvi.75.18.8624-
390 8638.2001 (2001).
391 23 Wang, S. W. *et al.* CCL5 and CCR5 interaction promotes cell motility in human osteosarcoma.
392 *PLoS One* **7**, e35101, doi:10.1371/journal.pone.0035101 (2012).
393 24 Shen, W. *et al.* Activation of the chemotactic peptide receptor FPRL1 in monocytes
394 phosphorylates the chemokine receptor CCR5 and attenuates cell responses to selected
395 chemokines. *Biochem Biophys Res Commun* **272**, 276-283, doi:10.1006/bbrc.2000.2770 (2000).
396 25 Moyer, J. R., Jr., Thompson, L. T. & Disterhoft, J. F. Trace eyeblink conditioning increases CA1
397 excitability in a transient and learning-specific manner. *J.Neurosci.* **16**, 5536-5546 (1996).
398 26 Oh, M. M., Oliveira, F. A. & Disterhoft, J. F. Learning and aging related changes in intrinsic
399 neuronal excitability. *Front Aging Neurosci* **2**, 2, doi:10.3389/neuro.24.002.2010 (2010).

400 27 Yokose, J. *et al.* Overlapping memory trace indispensable for linking, but not recalling, individual
401 memories. *Science* **355**, 398-403, doi:10.1126/science.aal2690 (2017).

402 28 Rogerson, T. *et al.* Molecular and Cellular Mechanisms for Trapping and Activating Emotional
403 Memories. *PLoS One* **11**, e0161655, doi:10.1371/journal.pone.0161655 (2016).

404 29 Mayford, M. & Reijmers, L. Exploring Memory Representations with Activity-Based Genetics.
405 *Cold Spring Harb Perspect Biol* **8**, a021832, doi:10.1101/cshperspect.a021832 (2015).

406 30 Tanaka, K. Z. *et al.* The hippocampal engram maps experience but not place. *Science* **361**, 392-
407 397, doi:10.1126/science.aat5397 (2018).

408 31 Mello, C. V. *et al.* Fat-storing multilocular cells expressing CCR5 increase in the thymus with
409 advancing age: potential role for CCR5 ligands on the differentiation and migration of
410 preadipocytes. *Int.J.Med.Sci.* **7**, 1-14 (2009).

411 32 Yung, R., Mo, R., Grolleau-Julius, A. & Hoeltzel, M. The effect of aging and caloric restriction on
412 murine CD8+ T cell chemokine receptor gene expression. *Immun Ageing* **4**, 8, doi:10.1186/1742-
413 4933-4-8 (2007).

414 33 Wilkin, T. J. & Gulick, R. M. CCR5 antagonism in HIV infection: current concepts and future
415 opportunities. *Annu Rev Med* **63**, 81-93, doi:10.1146/annurev-med-052010-145454 (2012).

416 34 Aharoni, D., Khakh, B. S., Silva, A. J. & Golshani, P. All the light that we can see: a new era in
417 miniaturized microscopy. *Nat Methods* **16**, 11-13, doi:10.1038/s41592-018-0266-x (2019).

418 35 Pnevmatikakis, E. A. & Giovannucci, A. NoRMCorre: An online algorithm for piecewise rigid
419 motion correction of calcium imaging data. *J Neurosci Methods* **291**, 83-94,
420 doi:10.1016/j.jneumeth.2017.07.031 (2017).

421 36 Zhou, P. *et al.* Efficient and accurate extraction of in vivo calcium signals from microendoscopic
422 video data. *Elife* **7**, doi:10.7554/eLife.28728 (2018).

423 37 Almeida-Filho, D. ConcatMiniscope: This is the first release of the ConcatMiniscope Pipeline
424 (Version 1.0.0-Beta) *Zenodo*, doi:10.5281/zenodo.5676164 (2021).

425 38 Friedrich, J., Zhou, P. & Paninski, L. Fast online deconvolution of calcium imaging data. *PLoS*
426 *Comput Biol* **13**, e1005423, doi:10.1371/journal.pcbi.1005423 (2017).

427 39 Wei, Z. *et al.* A comparison of neuronal population dynamics measured with calcium imaging
428 and electrophysiology. *PLoS Comput Biol* **16**, e1008198, doi:10.1371/journal.pcbi.1008198
429 (2020).

430

431

432
433
434
435
436
437
438
439
440
441
442
443
444
445
446
447
448
449
450
451
452
453
454
455
456
457
458
459
460
461
462
463
464
465
466
467
468
469
470
471
472
473
474
475
476
477

Methods

Animals

Ccr5 knockout (*Ccr5*^{-/-}) mice were purchased from Taconic Farms (Germantown, NY; B6.129P2-Ccr5tm1Kuz N10). Experimental WT, *Ccr5*^{+/-} and *Ccr5*^{-/-} mice (3 to 5 months old) were generated by intercrossing *Ccr5*^{+/-} mice. Littermates were used for *Ccr5* KO linking test. cFos-tTa mice that express tetracycline transactivator (tTA) protein under the control of the c-Fos (also known as Fos) promoter were maintained in a C57BL/6N background. *Ccl5* knockout (*Ccl5*^{-/-}) mice were purchased from Jackson lab (B6.129P2-Ccl5tm1Hso/J). 16-month-old male C57BL/6Nia were purchased from NIA for *Ccr5* expression detection and linking test. 11-week-old male C57BL/6N Tac mice were purchased from Taconic Farms (Germantown, NY) for all other experiments. Mice are housed in an AAALAC accredited facility with 12-12 light/dark cycles. Housing conforms to *The Guide for the Care and Use of Laboratory Animals*, 8th edition. The temperature setpoint is 72 degrees plus or minus 3 degrees; the humidity range is between 30% to 70%. All experiments were performed during the light phase of the cycle. All studies were approved by the Animal Research Committee at UCLA.

Viral constructs

Constructs for *iTango2* system were gifts from Hyungbae Kwon, which include pAAV-hSYN-DRD2-V2tail-TevN-BLITz1-TetR-VP16-bGHpA (Addgene plasmid #89874; <http://n2t.net/addgene:89874>; RRID:Addgene_89874), pAAV-hSYN-bArrestin2-TevC-P2A-TdTomato-WPRE-bGHpA (Addgene plasmid #89873; <http://n2t.net/addgene:89873>; RRID:Addgene_89873), pAAV-TRE-EGFP (Addgene plasmid #89875; <http://n2t.net/addgene:89875>; RRID: Addgene_89875), pTRE-EGFP (Addgene plasmid #89871; <http://n2t.net/addgene:89871>; RRID: Addgene_89871). pGP-CMV-NES-jRGECO1a was a gift from Douglas Kim & GENIE Project (Addgene plasmid # 61563; <http://n2t.net/addgene:61563>; RRID: Addgene_61563). pAAV.Syn.GCaMP6f.WPRE.SV40 was a gift from Douglas Kim & GENIE Project (Addgene viral prep # 100837-AAV1; <http://n2t.net/addgene:100837> ; RRID:Addgene_100837)

For the AAV-based shRNA construct for mouse CCR5, the target sequence (shCCR5) is 5'-GTGCAAGCTCAGTCTATACCTCAAGAGGGTATAGACTGAGCTTGCAC-3'.

The control sequence (shDsRed) is 5'-AGTTCCAGTACGGCTCCAAGAAGCTTGTTGGAGCGTACTGGAAC-3'.

For the Opto-CCR5 experiment, pLenti-Efl α -DIO-Opto-CCR5-EGFP was made by replacing the intracellular loops of rhodopsin with those of CCR5 to activate its specific intracellular signaling with light. The details of viral information are described in the Supplementary Table 1.

Real time-PCR

Total RNA was prepared using RNeasy Mini Kit (Qiagen, 74104) according to the manufacturer's instructions. Single-stranded cDNA was synthesized using SuperScript III First-Strand Synthesis SuperMix (Invitrogen, 18080400). Real-time PCR was performed with SYBR Green-based reagents (iQ SYBR Green Supermix; Bio-Rad, 1708880) using a LightCycler 480 II (Roche). The following are primers used for real-time PCR:

Mouse *ccr5*, 5'-GCTGCCTAAACCCTGTCATC-3' and 5'-GTTCTCCTGTGGATCGGGTA-3'

478 Mouse *ccl5*, 5'-TGCAGTCGTGTTTGTCACTC-3' and 5'-AGAGCAAGCAATGACAGGGA-3'
479 Mouse *ccl3*, 5'-TTCCACGCCAATTCATCGTT-3' and 5'-GCATTCAGTTCCAGGTCAGTG-3'
480 Mouse *ccl4*, 5'-CCTCCCCTCCTGCTGTTT-3' and 5'-GCTTGGAGCAAAGACTGCTG-3'
481 Mouse *36B4*, 5'-AGATGCAGCCAGATCCGCAT-3' and 5'-GTTCTTGCCCATCAGCACC-3'
482

483 ***In situ* hybridization**

484 Mouse brains were dissected and fast-frozen in OCT by dry Ice without PFA fixation. 20 μ m
485 frozen sections were sliced. In situ hybridization was performed using RNAscope Fluorescent
486 Multiplex Reagent Kit V1(ACD, 320850) and V2 (ACD, 323120) according to the manufacturer's
487 instructions. RNAscope Probe-Mm-Ccr5 (ACD, 438651) and Probe-Mm-Ccl5 was used to detect
488 *ccr5* and *Ccl5* mRNA. Probe-Mm-Rbfox3 (ACD, 313311) and Probe-Mm-Itgam (ACD, 469601)
489 were used as markers for neurons and microglia, respectively. Probe-Mm-*Slc17a7* (ACD, 416631)
490 and Probe-Mm-*Gad2* (ACD, 311491) were used as markers for excitatory and inhibitory neurons.
491 Probe-*mCherry* (ACD, 431201) and Probe-Mm-Fos (316921) were used for memory ensemble
492 labeling.
493

494 **Immunostaining**

495 Mice were transcardially perfused with 4% PFA (4% paraformaldehyde in 0.1 M phosphate buffer)
496 and after perfusion, brains were sliced coronally (50 μ m thick) with a vibratome and processed for
497 immunostaining. Primary antibodies, including chicken polyclonal anti-GFP (Abcam AB13970,
498 1:1000), mouse monoclonal anti-GFP (Synaptic Systems, 132 011, 1:500), Chicken anti-RFP
499 (Synaptic Systems, 409 006, 1:500), mouse anti-TetR Monoclonal Antibody (Clone 9G9, Takara,
500 63113, 1:500), mouse anti-NeuN (Chemicon, MAB377, 1:1000), rabbit anti-GFAP (Dako, Z0334,
501 1:500), rabbit anti-c-Fos (Cell Signaling, 9F6, #2250, 1:500), and rabbit anti-P2Y12 (AnaSpec,
502 AS-55043A, 1:1000) and secondary antibodies, including goat anti-chicken 488 (Invitrogen,
503 A11039, 1:2000), goat anti-mouse 488 (Invitrogen, A11029, 1:2000), goat anti-chicken 594
504 (Invitrogen, A11042, 1:2000), goat anti-rabbit 647 (Invitrogen, A21245, 1:2000) were used for
505 immunostaining. Brain slices were incubated with 4',6-diaminodino-2-phenylindole (DAPI,
506 Invitrogen, 1:2000) for 10 min and washed with PBS three times before mounting onto slides.
507 Immunostaining images were acquired by NIS-Elements AR (Nikon, v4.40.00) with a Nikon A1
508 Laser Scanning Confocal Microscope (LSCM). NIS-Elements AR Analysis (Nikon, v4.40.00) was
509 used to analyze the confocal images.
510

511 **Immunoblotting**

512 Cultured HEK 293 cells were lysed with RIPA buffer (Sigma, St. Louis, MO, R0278) with protease
513 inhibitor cocktail (Sigma, P8340), phosphatase inhibitor cocktail 2 (Sigma, P5726), phosphatase
514 inhibitor cocktail 3 (Sigma, P0044). Protein samples (10 μ g/well) were loaded to NuPAGE Novex
515 4–12% Bis-Tris protein gel (ThermoFisher Scientific, Carlsbad, CA, NP0336BOX) and
516 transferred onto polyvinylidene difluoride (PVDF) membranes. The membranes were then
517 blocked with 5% nonfat milk at room temperature for 1 hour and then probed with primary
518 antibodies (phospho-p44/42 MAPK, Cell Signaling 9101, 1:4000, dilution) at 4°C overnight.
519 Membranes were then incubated with HRP-conjugated secondary antibodies (goat anti-rabbit
520 HRP, Bio Rad, 170-6515, 1:5000) for 1 hour and developed with SuperSignal solutions (Thermo
521 Scientific). Then the membrane was stripped and probed again with primary antibodies (p44/42
522 MAPK, Cell Signaling 9102, 1:4000 dilution, β -actin 1:10,000, A5316, Sigma-Aldrich) and

523 secondary antibodies including goat anti-mouse HRP (Bio Rad, 170-6516, 1:10000) and goat anti-
524 rabbit HRP (Bio Rad, 170-6515, 1:5000),

525

526 **CCR5-*i*Tango2 system**

527 Inducible Tango2 (*i*Tango2) system is a genetic method of labeling and manipulating cells with
528 particular GPCR activation initially reported by Hyung-Bae Kwon lab¹⁹. Based on this method,
529 we designed CCR5-*i*Tango2. Briefly, it couples a tetracycline-controlled transcriptional activator
530 (tTA) to the C-terminal of mouse CCR5 via a specific tobacco etch virus protease (TEVp)-
531 sensitive cleavage site (TCS), which is protected by AsLOV2/*Ja* (light sensitive domain). Upon
532 activation, β -Arrestin tagged with TEVp-C (C-terminal region of TEVp) binds intracellular loop
533 of CCR5 tagged with TEVp-N (N-terminal region of TEV), which forms functional TEV and
534 cleave TEV-seq exposed to light stimulation. Then tTA is released and translocate into nucleus to
535 induce specific gene expression. To generate the CCR5-*i*Tango2 DNA constructs, full length
536 mouse CCR5 cDNA was sub-cloned into pAAV-hSYN-DRD2-V2tail-TevN-BLITz1-TetR-
537 VP16-bGHpA to replace DRD2 cDNA sequence (by VectorBuilder).

538 For analysis, ImageJ (v1.53f51) was used to quantify the EGFP and tdTomato intensity. Briefly,
539 EGFP cells were identified and outlined automatically (to create ROIs for EGFP⁺ counting) by
540 threshold imaging (threshold: 1.5-fold of the background intensity). Then, the intensity (gray
541 value) of the EGFP and tdTomato was measured by the software within the ROIs of identified
542 cells, and the EGFP/tdTomato ratio was calculated.

543

544 **Opto-CCR5 system**

545 Opto-XR is the genetically encoded optical tool designed by Karl Deisseroth lab²⁰, which can
546 control GPCR-initiated biochemical signaling pathways with high spatiotemporal precision.
547 Based on opto-XR, Won Do Heo lab designed and made the Opto-CCR5 construct and subclone
548 it into a lentivirus backbone (Lenti-Ef1a-DIO-Opto-CCR5-EGFP). Briefly, the intracellular loops
549 of rhodopsin were replaced with those of mouse CCR5. As a result, light induced structure change
550 of rhodopsin would activate intracellular CCR5 signaling.

551

552 **Stereotaxic Surgery**

553 Animals were anesthetized with 2% isoflurane and placed in a stereotaxic head frame on a heat
554 pad. Artificial tears were applied to the eyes to prevent eye drying. A midline incision was made
555 down the scalp, and a craniotomy was performed with a dental drill. After surgery, the animals
556 were subcutaneously injected with Carprofen (5 mg/kg) and Dexamethasone (0.2 mg/kg) before
557 recovery. Water with amoxicillin was applied for two weeks.

558 For cannula implantation, two guide cannulas (Plastics One, C313GS-5/SPC) were implanted
559 at the following coordinates relative to bregma (mm): 1) for dCA1, AP: -2.1, ML: \pm 1.7; 2) for
560 lateral ventricle, AP: -0.3, ML: \pm 1.0. Three weeks after cannulation, mice were anesthetized and
561 sterilized Veh or drug was infused into hippocampus through the internal cannula (Plastics One,
562 C313IS-5/Spc, 100nL/min) at DV: -1.6 mm (dCA1) or -2.5 mm (ventricle) relative to skull. After
563 infusion, the internal cannula was left in place for an additional 5 min to ensure full diffusion.
564 Drugs with the following concentration were infused: mouse CCL5 peptide (70nM in PBS, 1 μ L),
565 Maraviroc (10 mg/ml in saline with 7.5% beta-cyclodextrin, 1 μ L), DAPTA (50 nM in PBS, 1
566 μ L).

567 For virus injection, a Nanoliter injector (World Precision Instruments) was used to infuse virus
568 with Micro4 Controller (World Precision Instruments). Virus was infused at 50-100 nL/min. After

569 infusion, the capillary was kept at the injection site for 5 min and then withdrawn slowly. The
570 incision was closed with clips, which were removed 7 days later. The details of viruses used are
571 described in the Supplemental Information (Table S1).

572 For optical fiber implantation, fiber Optic Cannula (Newdoon, 200 μm , NA=0.37) was
573 immediately implanted after virus injection. The tip of the optic fiber was placed 600 μm above
574 the virus injection site. Then, the cannula was fixed with Metabond and dental cement.

575 For miniscope implantation, a GRIN lens was implanted into the dorsal hippocampal CA1
576 region as previously described¹. After GCaMP6f virus injection, a $\sim 2\text{mm}$ diameter circular
577 craniotomy was centered at the injection site. The cortex directly below the craniotomy was
578 aspirated with a 27-gauge blunt syringe needle attached to a vacuum pump. Cortex buffer (NaCl
579 135mM, KCL 5mM, CaCl₂ 2.5mM, MgSO₄ 1.3mM, HEPES 5mM, PH 7.4) was repeatedly applied
580 to the exposed tissue to prevent drying. The GRIN lens (0.50 NA, 2.0 mm in diameter, Grintech
581 GmbH) was slowly lowered above CA1 to a depth of 1.35 mm ventral to the surface of the skull at
582 the most posterior point of the craniotomy. Next, a skull screw was used to anchor the lens to the
583 skull. Both the lens and skull screw were fixed with super glue (Loctite, 45198) and dental cement
584 (Jet Denture Repair Package, Lang, 1223CLR). Low Toxicity Silicone Adhesive (Kwik-Sil, World
585 Precision Instruments) was used to cover the GRIN Lens for protection. Three weeks later, a small
586 baseplate was cemented onto the animal's head atop the previously formed dental cement.

587

588 **Memory ensemble labeling with cFos-tTA mice**

589 Adult male and female (3-8 months) cFos-tTa transgenic were bilaterally microinjected with 500 nl
590 of AAV1-TRE-mCherry into the dCA1. Mice were allowed to recover from surgeries for 3 weeks
591 and high doxycycline chow (1g/kg) was applied during the recovery. Mice were removed from
592 doxycycline chow and were fed with regular chow for 3 days before the behavior to allow the
593 tagging of neuronal ensemble for the memory linking experiments. The activity-dependent tagging
594 was shut off by administration of high dox chow 1h after behavioral tagging.

595

596 **Optogenetics**

597 For the CCR5-*iTango2* system, 3 weeks after virus injection and optic cannula implantation, the
598 mice were handled for 3 days and then habituated with the optic fiber connected in their home
599 cage for another 3 days (10min/day). Then the mice received contextual fear conditioning training
600 and returned to their home cage. After 2.5h, 5.5h, 11.5h and 23.5h, different groups of mice
601 received light stimulation in their home cage (473nm, 8-10mW, 10s on/50s off for 1h). The mice
602 were kept for another 48h for GFP expression before the brains were collected and fixed with PFA
603 perfusion. To validate CCR5-*iTango2* *in vitro*, HEK293 cells were transfected with *iTango2*
604 system constructs using Lipofectamine 2000 (Invitrogen, 11668027). One day later, light (473nm,
605 10s on/50s off for 1h) was delivered to the cells with/without CCL5 (1nM).

606 For Opto-CCR5, the mice were anesthetized with 1.5% isoflurane during light delivery (473nm,
607 $\sim 8\text{mW}$, 50s on/10s off for 30min). Then, the mice were returned to their home cage for 30 min to
608 recover before exposure to a different context. To validate Opto-CCR5 *in vitro*, HEK293 cells
609 were transfected with Opto-CCR5 construct using Lipofectamine 2000 (Invitrogen, 11668027).
610 One day later, light (473nm or 500nm, $\sim 1\text{-}2\text{ mW/mm}^2$, 2-5 min) was delivered to the cells to
611 activate Opto-CCR5.

612 For memory ensembles labeling with Chr2_{ETTC} pre-activation, 3 weeks after virus injection
613 and optic cannula implantation, the mice were handled for 3 days (2 min/day) and then habituated
614 to the experimental room and wearing optical fibers for another 3 days. For the pre-activation,

615 mice were connected to the optical fibers and returned to home cages for 5 min first, and then 3
616 min light stimulation (473nm, ~4-5mW, 10Hz, 20% duty cycle) was applied in home cage. After
617 light stimulation, optical fibers were disconnected and mice were allowed another 5 min recovery
618 in home cage before contextual fear conditioning.

619

620 **Memory linking with contextual fear conditioning**

621 The contextual memory linking task was carried out as previously described¹. Mice were first
622 handled for 3 days (1min/day) and then habituated to transportation and external environmental
623 cues for 2 minutes in the experimental room each day for another 3 days. In the contextual memory
624 linking task, mice explored 2 different contexts (A and then B, counterbalanced) which were
625 separated by 5h-7d. Mice explored each context for ten minutes. For immediate shock, mice were
626 placed in chamber B for 10 s followed by a 2s shock (0.65 mA). 58 seconds after the shock, mice
627 were placed back in their home cage. For the context tests, mice were returned to the designated
628 context. Freezing was assessed via an automated scoring system (Med Associates) with 30 frames
629 per second sampling; the mice needed to freeze continuously for at least one second before freezing
630 could be counted.

631

632 **Memory linking with place preference task**

633 Mice were gradually water restricted to 1.5-2.0 ml/day. Body weight was tightly monitored every
634 day to avoid a loss of over 15% of body weight. From the 3rd day of water restriction, mice were
635 handled for 5min/day for 3 days. Then mice were placed in the experimental room for 1h/day for
636 another 3 days for habituation. To test memory linking, mice were exposed to one of the two-
637 compartment apparatus (context A or context B, for each group the two contexts were counter
638 balanced) for 10 min, and 5h or 7d later, mice were placed in context C (with 1.5ml water
639 containing 0.2% saccharin) for 15min. One day later, mice were placed back to the two-
640 compartment apparatus and were allowed to freely explore the context A (pre-exposed context)
641 and context B (Novel context). The exploration was recorded and the time in each apparatus was
642 measured to examine the preference for each context.

643

644 **Slice preparation and CCL5 treatment**

645 Adult mice (3-6 months old) were deeply anesthetized with isoflurane and the brains were rapidly
646 dissected out and transferred to oxygenated (95% O₂/5% CO₂), ice-cold cutting solution
647 containing 92 mM NaCl, 2.5 mM KCl, 1.25 mM NaH₂PO₄, 30 mM NaHCO₃, 20 mM HEPES,
648 25 mM glucose, 2 mM Thiourea, 5m M Na-ascorbate, 3 mM Na-pyruvate, 2 mM CaCl₂, and 2
649 mM MgCl₂. Coronal slices (400 μm thick) containing the hippocampus were cut using a Leica
650 VT1200 vibrating blade microtome, transferred to a submerged holding chamber containing
651 oxygenated cutting solution and allowed to recover for 1h at room temperature. Prior to performing
652 whole-cell recordings, each slice was incubated in a separate chamber containing either
653 oxygenated aCSF (containing 115 mM NaCl, 10 mM glucose, 25.5 mM NaHCO₃, 1.05 mM
654 NaH₂PO₄, 3.3 mM KCl, 2 mM CaCl₂, and 1 mM MgCl₂) or 10nM CCL5 in oxygenated aCSF
655 for 1h. Following incubation, slices were immediately transferred to a superfused recording
656 chamber and constantly perfused with oxygenated aCSF maintained at 28°C. All recordings were
657 performed within 30 min of aCSF or CCL5 incubation.

658

659 **Whole-cell patch recordings**

660 Whole cell current-clamp recordings were performed on pyramidal neurons in the CA1 region of
661 the hippocampus using pipettes (3-5MΩ resistance) pulled from thin-walled Borosilicate glass
662 using a Sutter P97 Flaming/Brown micropipette puller and filled with an internal solution
663 containing 120 mM K-methylsulfate, 10 mM KCl, 10 mM HEPES, 10 mM Na-phosphocreatine,
664 4 mM Mg-ATP, and 0.4 mM Na-GTP. All recordings were obtained using a MultiClamp 700B
665 amplifier controlled by the pClamp 10 software and digitized using the Digidata 1440A system.
666 Signals were filtered at 10 kHz and digitized at 20 kHz. Neurons were included in the study only
667 if the initial resting membrane potential (Vm) < -55 mV, access resistance (Ra) was < 20MΩ, and
668 were rejected if the Ra changed by >20% of its initial value. For all recordings, neurons were held
669 at -65 mV. The stable resting membrane potential of neurons was measured and averaged over a
670 60s duration with 0 mA current injection immediately after breaking in. To investigate the firing
671 rate of neurons, the number of action potentials fired in response to a 600 msec pulse of
672 depolarizing current injection (0 pA to 380 pA in 20 pA increments) was calculated. Three pulses
673 were delivered for each current amplitude and the average number of action potentials fired for
674 each current amplitude was plotted. The recordings were analyzed using Stimfit 0.15.8 and the
675 data were screened for statistical outliers ($\pm 2SD$).

676

677 **Miniscope data acquisition and analyses**

678 One-photon calcium imaging was recorded using UCLA miniscopes³⁴. During recordings, digital
679 imaging data were sent from the CMOS imaging sensor (Aptina, MT9V032) to custom data
680 acquisition (DAQ) electronics and USB Host Controller (Cypress, CYUSB3013) over a light-
681 weight, highly flexible co-axial cable. Images were acquired at 30 frames per second, using display
682 resolution at 752 x 480 pixels (1 pixel = 1-2μm), and saved into uncompressed avi files. The
683 analysis pipeline was written in MATLAB using first the NoRMCorre algorithm for motion
684 correction (rigid registration)³⁵, followed by individual neuron identification and extraction using
685 the CNMF-E algorithm³⁶. During motion correction, videos were 2x spatially down-sampled using
686 the default built-in NoRMCorre protocol. During CNMF-E initialization, videos were further 2x
687 spatially down-sampled and 5x temporally down-sampled. The quality of neuron extraction was
688 verified using a MATLAB custom-made Neuron Deletion GUI. We excluded the detected putative
689 neurons exhibiting ROI morphology or calcium trace abnormalities or incoherencies between the
690 calcium trace peaks and the expected correspondent fluorescence increases in the video, and the
691 neuron deletion was performed by experimenters blinded of the experimental groups and
692 conditions. Each 10-min video from individual sessions was analyzed separately. Recordings from
693 multiple sessions of the same animal were aligned using the spatial foot prints (neuron.A, output
694 from CNMF-E) of each one of the detected cells for individual sessions. The centroid distance and
695 spatial correlation were calculated for all cell pairs. Cell pairs from different sessions were
696 considered to match if their spatial correlation ≥ 0.8 and their centroid distance ≤ 5 pixels.
697 Overlapping percentages between two given sessions were calculated as the number of matched
698 cells over the average of the total number of detected cells in each one of the two sessions.
699 Overlapping Index = $Ctx A^+ Ctx B^+ cell (Overlap) / [(Ctx A^+ cell + Ctx B^+ cell) / 2] \%$.

700

701 We reanalyzed our miniscope data using a MATLAB custom-made concatenation analysis
702 pipeline³⁷ to identify, track, and analyze the activity of individual neurons across sessions. Briefly,
703 the motion-corrected videos (as described above), from context exposure sessions of individual
704 animals, were aligned and concatenated into a long video. The long video was then processed
705 through CNMF-E using the same parameters described above to extract putative neurons. After

706 deletion of false-positive ROIs using the Neuron Deletion GUI protocol described above, we
707 projected the raw calcium trace of the remaining ROIs for each session separately using the
708 CNMF-E algorithm. Finally, we inferred spike activity from raw calcium traces from individual
709 sessions using the Foopsi Thresholded algorithm³⁸, and we binarized neuronal activity (NA) from
710 individual frames into 1 (active frame) and 0 (inactive frame). We calculated interevent intervals
711 (IEI) as the time interval between consecutive active frames from individual sessions (Extended
712 Fig. 8). The cumulative distribution of IEIs was first calculated for each individual neuron, then
713 averaged across neurons to represent individual animals. Finally, the single animal values were
714 averaged to depict group results (Extended Fig. 8c, d, g). We defined subsets of neurons based on
715 their average NA by calculating the number of active frames for each neuron within specific
716 sessions and sorting cells from highest to lowest NA (e.g., Top 10%, as in Extended Fig. 9b) or
717 from lowest to highest NA (e.g., Bottom 10%, as in Extended Fig. 9c). The coefficient of variation
718 for each neuron in a specific session was defined as the ratio between the standard deviation of the
719 IEI distribution and the average NA within that session. We validated the usage of IEI from
720 calcium imaging as a significantly reliable representation of inter-spike interval (ISI) from in-vivo
721 electrophysiology recordings (ephys) by leveraging a dataset containing simultaneous GCaMP6f
722 calcium imaging and loose-seal cell-attached electrical recordings of cortical neuronal activity³⁹.
723 ISIs were defined by the time interval between consecutive spikes and the coefficient of variation
724 for ephys recordings was calculated the same way as in calcium imaging recordings using the ISI
725 distribution instead of the IEI distribution.

726 We defined the probability of overlap based on average NA by calculating the probability of a
727 subset of neurons from Ctx A (e.g., Top 10% NA) to have a specific relative level of NA (e.g., be
728 within the Top 30% NA) in Ctx B. This was mathematically defined as in the example: $P_{A10,B30} =$
729 $\frac{N_{A10,B30}}{U}$, where $P_{A10,B30}$ is the probability of the Top 10% NA in Ctx A (A10) to be within the Top
730 30% NA in Ctx B (B30); $N_{A10,B30}$ is the actual number of neurons lying within A10 and B30, and
731 U is the universe of all cells detected from all sessions by the analysis using the concatenated long
732 video. The probability values were normalized by chance through the calculation of the ratio
733 between $P_{A10,B30}$ and $P_{A10} \times P_{B30} (= 0.1 \times 0.3)$ (Extended Fig. 9b-d). For plots on Extended Fig.
734 9b,c (X axis), the same percentage values were used for contexts A and B (e.g.,
735 $P_{A10,B10}, P_{A20,B20}, \dots$). We have also calculated $P_{A10,B10}$ between different subsets of 10% cells from
736 Ctx A and the Top 10% NA cells from Ctx B (Extended Fig. 9e). We have spanned all cells from
737 Ctx A, from highest to lowest NA, with a sliding window of size = 10% and step = 2% (Extended
738 Fig. 9e, X axis). To express the significance of the probability of overlap values, they were
739 represented as standard deviations from the mean of a null distribution created by randomly
740 subsampling (10,000 times) 10% cells from Ctx A followed by the calculation of $P_{A10,B10}$, in which
741 B10 is the Top 10% NA from Ctx B.

742

743 **Colocalization calculation**

744 Different calculations were applied to reflect colocalization between protein or mRNA
745 distributions. For overlap between c-Fos and Opto-CCR5/ChR2_{ETTC}/CCR5-*i*Tango2/shCCR5,
746 chance level = (c-Fos⁺/DAPI)*(EGFP⁺/DAPI)%, colocalization = [(c-Fos⁺EGFP⁺/DAPI)%
747 /Chance level]%, distribution index = [a/(a+b)]%, a = (c-Fos⁺EGFP⁺/EGFP⁺)%, b = (c-Fos⁺EGFP⁻
748 /EGFP⁻)%, EGFP⁺, c-Fos⁺ and EGFP⁺ indicate the number of cells with positive signal

749 respectively. Opto-CCR5, CCR5-*i*Tango2 and shCCR5 had EGFP as the reporter while Chr2_{ETTC}
750 was tagged with mCherry instead. For overlap among *Ccr5*, *mCherry* and *c-Fos* mRNA,
751 overlapping probability (over chance) = (a-b)/b, a = (*mCherry*⁺*c-Fos*⁺/DAPI)% (which is the
752 observed overlap%), b = [(*mCherry*⁺/DAPI)*(*c-Fos*⁺/DAPI)]% (which is the overlap chance%).

753

754 **Statistics and reproducibility**

755 The investigators who collected and analyzed the data including behavior, miniscope,
756 electrophysiological and staining were blinded to the mouse genotypes and treatment conditions.
757 Error bars in the figures indicate the SEM. All statistical analyses were performed using GraphPad
758 Prism 6. For behavior experiments, n designates the number of mice. For biochemical experiments,
759 n designates the number of brains or cells collected. For electrophysiological measurements, n
760 designates the number of neurons. All statistical tests are two-sided. Statistical significance was
761 assessed by Student's t test, Kolmogorov–Smirnov test or one- or two-way ANOVA where
762 appropriate, followed by the indicated post hoc tests for repeated measures. Significance levels
763 were set to P = 0.05. Significance for comparisons: *P < 0.05; **P < 0.01; ***P < 0.001. The
764 details of statistical information are described in the Supplementary Table 2.

765

766 Representative histological images were repeated independently in different mice with similar
767 results for Fig. 1d (n ≥ 4 per group), Fig. 1h (n = 3 per group), Fig. 1i (n ≥ 5 per group), Fig. 2d and f
768 (n = 6), Fig. 3c (n ≥ 3 per group), Fig. 3f (n = 6), Fig. 4c (n ≥ 4 per group) and Fig. 4e (n = 5 per group),
769 and Extended Data Fig. 1e (n ≥ 3 per group), Extended Data Fig. 1e (n ≥ 3 per group), Fig. 1g (n = 5
770 per group), Extended Data Fig. 2a (n = 5), Extended Data Fig. 2d (n = 4), Extended Data Fig. 2h (n = 4
771 per group), Extended Data Fig. 3l (n ≥ 3 per group), Extended Data Fig. 4b (n = 3 per group),
772 Extended Data Fig. 4e (n ≥ 3 per group), Extended Data Fig. 4h (n ≥ 4 per group) Extended Data
773 Fig. 5f (n = 4), Extended Data Fig. 7a (n = 8) and Extended Data Fig. 7d (n = 4 per group).
774 Representative in vitro images were biologically duplicated.

775

776

777 **Extended Data Figures**

778

779 **Extended Data Fig. 1 | Dorsal hippocampal expression of CCR5 and its ligands after fear** 780 **conditioning.**

781 **a**, Schematics of hippocampal tissue collection.

782 **b-d**, qPCR experiment to measure *Ccl3* (**b**), *Ccl4* (**c**), and *Ccl11* (**d**) expression in naïve mice (HC)
783 and in mice at different times after contextual fear conditioning. HC=home cage. HC n=6, 3 h n=2,
784 6 h n=8, 12 h n=7, 24 h n=8 mice.

785 **e**, Representative images of *Ccr5*, *Slc17a7* (excitatory neuronal marker), and *Gad2* (inhibitory
786 neuronal marker) mRNA expression in dCA1 from naïve mice or mice 3-24h after fear
787 conditioning. Red arrows: cells expressing *Ccr5* and *Slc17a7*. Orange arrows: cells expressing
788 *Ccr5* and *Gad2*. Scale bar, 50 μm.

789 **f**, Number of *Ccr5*-expressing excitatory and inhibitory neurons 3-24h after fear conditioning (HC
790 n=4, 3 h n=4, 6 h n=4, 12 h n=4, 24 h n=3 mice; **P < 0.01, ***P < 0.001, two-way repeated
791 measures ANOVA).

792 **g**, Representative images of *Ccl5*, *Itgam*, and *Rbfox3* mRNA expression in dCA1 from naïve mice
793 or mice 3-24h after fear conditioning. Red arrows: cells expressing *Ccl5* and *Itgam*. Orange
794 arrows: cells expressing *Ccl5* and *Rbfox3*. Scale bar, 50 μm.

795 **h**, Number of *Ccl5*-expressing microglia and neurons in naïve mice (n=5 mice; **P* < 0.05, paired
796 t-test).

797 **i**, Number of *Ccl5*-expressing microglia and neurons in HC mice and 3-24h after fear conditioning
798 (n=5 mice per group; *****P* < 0.0001, two-way repeated measures ANOVA).

799 All results shown as mean ± s.e.m.

800

801 **Extended Data Fig. 2 | The co-localization of *Ccr5* expression and memory ensembles**
802 **measured with cFos-tTA mice and the optogenetic (ChR2_{ETTC}) pre-activation system.**

803 **a**, Representative images of *Ccr5* and *mCherry* (neuronal ensemble) mRNA expression in dCA1
804 from cFos-tTA mice 6h after fear conditioning. Co-localization was labeled with dashed circles.
805 Scale bar, 20 µm.

806 **b**, Quantification of *Ccr5* expression in total cells (DAPI) and neuronal ensemble (*mCherry*⁺).
807 (n=5 mice; **P* < 0.05, paired t-test).

808 **c**, Schematics to use blue light to activate ChR2_{ETTC}-expressing neurons to be involved in neuronal
809 ensemble by pre-activation. INTRSECT system (Cre-off/Flp-on) was used to label non-ChR2_{ETTC}-
810 expressing neurons as the control.

811 **d**, Representative images of *mCherry* (pre-activated neurons), c-Fos (neuronal ensembles), and
812 EYFP (non-preactivated neurons) in dCA1 24h after the novel context exposure. Scale bar, 50 µm.

813 **e**, c-Fos distribution in *mCherry*⁺, EYFP⁺ or non-infected cells.

814 **f**, Quantification of the colocalization between c-Fos and *mCherry* or EYFP. Colocalization (of c-
815 Fos and *mCherry*) = (c-Fos⁺*mCherry*⁺/DAPI)/[(c-Fos⁺/DAPI)*(*mCherry*⁺/DAPI)] (n=4 mice per
816 group; ***P* < 0.01, paired Student's t-test).

817 **g**, Schematics to detect the colocalization of *Ccr5* expression in neuronal ensembles using pre-
818 activation system.

819 **h**, Representative images of *Ccr5* and *mCherry* (neuronal ensemble) mRNA expression in dCA1
820 of cFos-tTA mice 6h after fear conditioning. Colocalization was labeled with dashed circles. Scale
821 bar, 20 µm.

822 **i**, Quantification of *Ccr5* expression in total cells (DAPI) and neuronal ensemble (*mCherry*⁺) (n=4
823 mice per group; **P* < 0.05, ***P* < 0.01, two-way repeated measures ANOVA).

824 All results shown as mean ± s.e.m.

825

826 **Extended Data Fig. 3 | Characterization of CCR5-*i*Tango2.**

827 **a**, Schematics of CCR5-*i*Tango2 constructs.

828 **b, c**, Expression validation of the CCR5-*i*Tango system in HEK-293 cells. DRD2-*i*Tango2 (for
829 Dopamine 2 receptor) was used as a positive control. **b**, Representative images of tTA
830 immunostaining. Scale bar, 50 µm. **c**, Quantification of tTA expression (intensity normalized to
831 DAPI). n=3 slides per group; **P* < 0.05, one-way ANOVA.

832 **d**, HEK-293 cells were transfected with 3 plasmids (see methods) for 24h and then treated with 10
833 nM CCL5 and blue light to induce EGFP expression.

834 **e**, Representative images of EGFP expression after different treatments. Scale bar, 50 µm.

835 **f**, Quantification of EGFP and tdTomato ratio (intensity). Light⁻CCL5⁻ n=70, Light⁺CCL5⁻ n=97,
836 Light⁻CCL5⁺ n=97, Light⁺CCL5⁺ n=282 cells; *****P* < 0.0001, one-way ANOVA. Compared to
837 control, light or CCL5 group, only the group with both light and CCL5 showed EGFP expression.

838 **g**, Light power-dependent EGFP expression. Results were normalized to no light control (30
839 mW/mm² n=320, 90 mW/mm² n=307 cells; *****P* < 0.0001, student's t-test).

840 **h**, Duty cycle dependent EGFP expression. The light stimulation was delivered every minute
841 (~0.017 Hz) to induce EGFP expression. Light was kept on for 10-60 s during each stimulation to
842 induce EGFP expression (10 s/min n=282, 20 s/min n=253, 30 s/min n=282, 40 s/min n=319, 50
843 s/min n=307, 60 s/min n=441 cells).

844 **i**, Dose curve of CCL5 to induced CCR5 activation (measured by EGFP/tdTomato fluorescence
845 ratio) in cultured HEK-293 cells (10^{-12} M n=49, 10^{-11} M n=39, 10^{-10} M n=29, 10^{-9} M n=77, 10^{-8} M
846 n=86 cells).

847 **j**, Time course of EGFP expression. The green fluorescence increased monotonically during the
848 different time intervals investigated. Compared to other time intervals (2, 4, 6, 8 and 24h), the 48h
849 time interval showed the highest EGFP/tdTomato ratio (Light⁺CCL5⁺ 0 h n=58, 2 h n=194, 4 h
850 n=282, 6 h n=310, 8 h n=316, 24 h n=396, 48 h n=345 cells; Light⁻CCL5⁻ 2 h n=195, 4 h n=219,
851 6 h n=290, 8 h n=304, 24 h n=445, 48 h n=401 cells; * $P < 0.05$, **** $P < 0.0001$, two-way ANOV-
852 A).

853 **k**, Schematics of CCR5-*i*Tango2 AAVs injected into mouse hippocampus and validated through
854 intra-hippocampal infusion of CCL5 and fiber-optic light stimulation.

855 **l**, Representative images of CCR5-*i*Tango2-expressing hippocampal dentate gyrus neurons in
856 control condition (no light and CCL5), light only, and light with CCL5. Ligand and light were
857 directly delivered into the hippocampus. Scale bar, 250 μ m.

858 **m**, Left: To test CCR5-*i*Tango2 activation in dCA1 (Fig. 1h), CCL5 was infused into the lateral
859 ventricle (LV) while light was delivered into dCA1 of hippocampus (HPC). Right: Schematics of
860 CCR5-*i*Tango2 AAVs.

861 All results shown as mean \pm s.e.m.

862

863 **Extended Data Fig. 4 | CCR5 activation measured with the CCR5-*i*Tango2 system *in vivo*.**

864 **a-c**, Validation of the leakage in CCR5-*i*Tango2 system *in vivo*.

865 **a**, Schematics to test the CCR5-*i*Tango2 system without light activation.

866 **b**, Representative images of EGFP and CCR5-*i*Tango2-expressing dCA1 neurons after fear
867 conditioning. Scale bar, 50 μ m.

868 **c**, Quantification of EGFP expression (intensity normalized to tdTomato which is tagged to β -
869 Arrestin through P2A, reflecting expression of the *i*Tango system (n=3 mice per group).

870 **d-f**, Validation of the maraviroc mediated CCR5 inhibition *in vivo*.

871 **d**, Maraviroc was co-infused with CCL5 into mouse dCA1. The CCR5-*i*Tango2 was used to
872 measure CCR5 activation *in vivo*.

873 **e**, Representative images of CCR5-*i*Tango2-expressing dCA1 neurons after fear conditioning.
874 Scale bar, 50 μ m.

875 **f**, Quantification of EGFP expression in different treatment (n=3 mice per group; * $P < 0.05$, one-
876 way ANOVA).

877 **g-i**, Analyses of colocalization of c-Fos and CCR5 activation.

878 **g**, Schematics to test c-Fos expression in EGFP⁺ cells after learning with the CCR5-*i*Tango2
879 system.

880 **h**, Representative images of colocalization between EGFP and c-Fos in dCA1. Red arrows: c-
881 Fos⁺EGFP⁺ cells. Scale bar, 50 μ m.

882 **i**, Percentage of c-Fos⁺EGFP⁺ cells in total cells (6 h n=6, 12 h n=4, 24 h n=5 mice; * $P < 0.05$,
883 two-way repeated measures ANOVA).

884 All results shown as mean \pm s.e.m.

885

886 **Extended Data Fig. 5| Characterization of Opto-CCR5.**

887 **a**, HEK-293 cells were transfected with Opto-CCR5 and jRGECO1a (Calcium sensor with red
888 fluorescence) for 24h and then stimulated with blue light to induce a calcium response.

889 **b**, Representative images at 0 min or 2 min after stimulation, or in the medium with high calcium
890 concentration. Scale bar, 20 μm .

891 **c**, Quantification of fluorescence change after light stimulation. In HEK-293 cells, Opto-CCR5-
892 EGFP activation by light significantly increased intracellular Ca^{2+} concentration reflected by
893 jRGECO1a (Control 2 min n=95, Control 5 min n=96, Opto-CCR5 2 min n=86, Opto-CCR5 5 min
894 n=89 cells; $**P < 0.01$, two-way ANOVA).

895 **d, e**, Opto-CCR5 activation increased pErk1/2 in HEK-293 cells.

896 **d**, HEK-293 cells were transfected with the Opto-CCR5 construct. After 24h expression, the cells
897 were starved in HEPES buffer for 1h before a 2min light stimulation to reduce basal pErk1/2 levels.

898 **e**, Cells were collected at 0 (no light stimulation), 15, 30 or 60 min after light stimulation and
899 subjected to Western blot analysis.

900 **f**, Expression of Opto-CCR5 in dCA1 neurons. To express Opto-CCR5 in dCA1 neurons, AAV1-
901 hSyn-Cre was co-injected with Lenti-DIO-Opto-CCR5. NeuN (neuron marker), GFAP (astrocyte
902 marker) and P2Y12 (microglia marker) were co-stained with EGFP in dCA1. Scale bar, 20 μm .

903 All results shown as mean \pm s.e.m.

904

905 **Extended Data Fig. 6| CCR5/CCL5 signaling regulates memory linking in an appetitive**
906 **place preference task.**

907 **a-f**, Place preference-based behavior model to test the linking of contextual memories.

908 **a**, Schematics of place preference-based linking behavior.

909 **b**, Representative trajectory plot (in the 3rd minute) of mice in the pre-exposed context and a novel
910 context with a 5h and 7d interval.

911 **c, d**, Mice showed a significant preference for pre-exposed context during the 3rd minute in the 5h
912 group compared to the 7d group (5h, n=13, 7d n=12; $*P < 0.05$, one sample paired t-test compared
913 to 50%)

914 **e**, Representative trajectory plot (in the 3rd minute) of mice in the pre-exposed context and a novel
915 context with Vehicle or CCL5 infusion.

916 **f**, CCL5 infusion in dCA1 impaired contextual memory linking with a 5h interval (Veh n=7, CCL5
917 n=8; $*P < 0.05$, one sample paired t-test compared to 50%).

918 **g**, *Ccl5* knockout extended the temporal window of contextual memory linking (WT n=11, *Ccl5*^{-/-}
919 n=16; $*P < 0.05$, $**P < 0.01$, two-way repeated measures ANOVA).

920 All results shown as mean \pm s.e.m.

921

922 **Extended Data Fig. 7| CCR5 regulate memory allocation.**

923 **a, b**, *Ccr5* knockdown enhanced memory allocation.

924 **a**, Schematics of AAV8-shRNA-CCR5-Efl α -EGFP injection, and representative images of c-Fos
925 and EGFP staining. Two EGFP⁺c-Fos⁺ were labelled by dotted line circle and two EGFP⁺c-Fos⁻
926 were labelled by asterisk. Scale bar, 20 μm .

927 **b**, dCA1 neurons with *Ccr5* knockdown had a higher probability of expressing c-Fos after a
928 memory test in context A. Left: The percentage of c-Fos⁺EGFP⁺ cells in total (DAPI). Chance
929 level was calculated as (c-Fos⁺/DAPI)*(EGFP⁺/DAPI); right: percentage of c-Fos⁺ cells in non-
930 EGFP cells (Con) or in EGFP⁺ cells with *Ccr5* knockdown (shCCR5) (n=8, $**P < 0.01$, paired t-
931 test).

932 **c-h**, Expression of c-Fos and Opto-CCR5 or EGFP control in dCA1.
933 **d**, Representative images of colocalization between c-Fos and EGFP control after light stimulation
934 and novel context exposure. Scale bar, 50 μ m.
935 **e**, Colocalization between c-Fos⁺ cells and EGFP⁺ cells after normalization to chance level. Chance
936 level = (c-Fos⁺/DAPI)*(EGFP⁺/DAPI)%. n=4.
937 **f**, Quantification of c-Fos distribution in EGFP⁺ and non-EGFP cells in the Opto-CCR5-EGFP or
938 EGFP control group. Distribution index = (c-Fos⁺EGFP⁺/EGFP⁺)/(c-Fos⁺EGFP⁺/EGFP⁺ + c-
939 Fos⁺EGFP⁻/EGFP⁻)% (0 mW n=13, 2 mW n=3, 4 mW n=5, 8 mW n=3; **P* < 0.05, ***P* < 0.01,
940 one-way ANOVA).
941 **g**, Percentage of c-Fos positive cells (normalized to cells with DAPI staining) in dCA1 with light
942 stimulation of different power levels.
943 **h**, Percentage of EGFP expression cells (normalized to cells with DAPI staining) in dCA1 with
944 light stimulation of different power levels.
945 All results shown as mean \pm s.e.m.

946

947 **Extended Data Fig. 8 | Analysis of the cumulative distribution of inter-event intervals**
948 **recorded with miniscopes in WT and *Ccr5* KO mice.**

949 **a**, Schematics used to extract spike information from raw traces of calcium imaging. Plot shows a
950 3s chunk of data from a single neuron using GCaMP6f calcium imaging and loose-seal cell-
951 attached electrophysiological (Ephys) recordings.

952 **b**, The average inter-event interval (IEI, from miniscope recordings) is highly correlated with the
953 average inter-spike interval (ISI, by Ephys) (n=36 cells; $R^2=0.92$, *P* < 0.0001, $\rho=0.96$, Pearson's
954 correlation coefficient).

955 **c**, Cumulative distribution of IEI of the top 10% most active neurons (in Ctx A). The top 10% most
956 active neurons from WT mice showed a significantly different distribution of IEI 5h compared to
957 2d after the context A exposure. In contrast, this subset of cells showed a similar pattern for both
958 time intervals in *Ccr5*^{-/-} mice (WT mice n=5, *Ccr5*^{-/-} mice n=6; *****P* < 0.0001, Kolmogorov-
959 Smirnov test).

960 **d**, Cumulative distribution of IEIs of the top 10% most active neurons and the remaining 90%
961 neurons (in Ctx A) at 5h or 2d after the context A exposure (WT n=5, *Ccr5*^{-/-} n=6).

962 **e**, Although neurons may have similar number of spikes during a certain time period of recording,
963 the difference of their coefficient of variation unveils different firing patterns ranging from regular
964 firing (Cell 1) to bursty firing (Cell 2).

965 **f**, The coefficient of variation of IEI (by calcium imaging) highly correlates with the coefficient of
966 variation of ISI (by Ephys) (n=36 cells; $R^2=0.38$, *P*=0.0001, $\rho=0.61$, Pearson's correlation
967 coefficient).

968 **g**, Cumulative distribution of IEI (the first 5s, zoom-in from **d**) of the top 10% highly active
969 neurons and the remaining 90% neurons (in Ctx A) at 5h or 2d after the context A exposure. The
970 difference between the top 10% most active and the remaining 90% neurons in Ctx A was strongly
971 reduced from 5h to 2d in WT mice but not in *Ccr5*^{-/-} mice (WT n=5, *Ccr5*^{-/-} n=6).

972 **h**, Coefficient of variation from the top 10% most active neurons (normalized to the remaining
973 90%). WT or *Ccr5*^{-/-} mice were exposed to Ctx B 5h or 2d after Ctx A. WT mice showed a
974 significant decrease in the coefficient of variation of IEI comparing the data for the 2d and 5h
975 intervals, while *Ccr5*^{-/-} mice had similar coefficient of variation of IEI in both intervals (WT n=5,
976 *Ccr5*^{-/-} n=6; **P* < 0.05, two-way repeated measures ANOVA).

977 All results shown as mean \pm s.e.m.

978

979 **Extended Data Fig. 9 | Analysis of neuronal activity and overlap probability in WT and**
980 ***Ccr5* KO mice.**

981 **a**, Schematics showing that cells in neuronal ensembles can be sorted into cells with high neuronal
982 activity (red) and low activity (blue), based on their average activity during the exploration of Ctx
983 A and Ctx B which were separated by either a 5h or 2d interval.

984 **b, c**, Left: Probability of overlap (averaged across mice) between subsets of cells with different
985 levels of activity (Y axis) during exploration of Ctx A and Ctx B, in WT and *Ccr5*^{-/-} mice across
986 time in Ctx B (X axis). Color bars refer to normalized probabilities (chance=1). Cumulative values
987 were used for x and y axis (e.g., for x axis, 200s means 0-200s; for y axis, 30 refers to the neurons
988 within the top 30% of high (**b**) or low (**c**) activity). Right: the distribution of SEM across mice for
989 the figures on the left. Asterisks (in the probability of overlap figures) represent the maximum
990 SEM from each plot (WT mice n=5, *Ccr5*^{-/-} mice n=6).

991 **b**, Probability of overlap between high activity cells in Ctx A and high activity cells in Ctx B in
992 WT and *Ccr5*^{-/-} mice. Note that the top 10% high activity cells in Ctx A are very likely to remain
993 within the top 10% high activity cells in Ctx B 5h later for both WT and *Ccr5*^{-/-} mice. In contrast,
994 this subset of cells was reactivated around chance levels 2d later in Ctx B in WT mice, but not in
995 *Ccr5*^{-/-} mice. In the *Ccr5*^{-/-} mice this subset of cells was still very likely to remain within the top
996 10% high activity cells in Ctx B.

997 **c**, Probability of overlap between low activity cells in Ctx A and high activity cells in Ctx B in WT
998 and *Ccr5*^{-/-} mice. In contrast to high activity cells in Ctx A, the low activity cells in Ctx A were
999 less likely (compared to chance) to be within the high activity cells in Ctx B.

1000 **d**, The probability of overlap between different ensembles (Ctx A and Ctx B) was sorted by
1001 neuronal activity in Ctx A and Ctx B, with a 5h or 2d interval between the two contextual
1002 exposures. Cells were sorted in percentages from top to bottom mean neuronal activity in the first
1003 context (Ctx A, y axis) and from left to right in the second context (Ctx B, x axis). With a 5h
1004 interval between Ctx A and B, the likelihood that neurons with high activity in Ctx A remained
1005 with high activity in Ctx B was higher than chance for both WT and *Ccr5* KO mice. With a 2d
1006 interval, the likelihood that neurons with high activity in Ctx A remained high activity in Ctx B
1007 was at chance levels in WT mice. In contrast, *Ccr5* KO mice showed a pattern similar to that
1008 observed with the 5h interval (WT mice n=5, *Ccr5*^{-/-} mice n=6).

1009 **e**, Cells were again sorted from high to low activity in Ctx A with a 10% sliding window and 2%
1010 steps. The probability of overlap between subsets of cells (10% ensemble size) from Ctx A and
1011 the ensemble cells with top 10% high activity in Ctx B was plotted. The probability values were
1012 z-scored with respect to a null distribution created by randomly subsampling 10% of cells from
1013 Ctx A 10,000 times (i.e., results are represented as standard deviation (SD) from the mean of the
1014 null distribution). The 2SD threshold is labeled with a dashed line (WT mice n=5, *Ccr5*^{-/-} mice
1015 n=6).

1016

1017 **Extended Data Fig. 10 | Graphic abstract.**

1018 **a**, In young mice, CCR5 signaling increases at a time point more than 5h after learning, and
1019 neuronal excitability and memory ensemble overlap remain high at 5h after learning. As a result,
1020 memories for context A (neutral context) and context B (shocked context) are linked together, and
1021 mice show high freezing during the test in context A.

1022 **b**, In aged mice, CCR5 signaling is higher than young mice at baseline and there is a further
1023 increase before 5h after learning, which lead to a reduction of neuronal excitability and memory

1024 ensemble overlap at 5h after learning. As a result, memories for context A (neutral context) and
1025 context B (shocked context) are not linked, and mice show low freezing during the test in context
1026 A.

1027
1028 **Acknowledgements** We thank A. Macalino, E. Chen, E. Ramirez, C. Riviere-Cazaux, M. López-
1029 Aranda and E. Lu for advice and technical support and M. Sehgal and LM. De Biase for providing
1030 transgenic mice. This work was supported by grants from the NIMH (R01 MH113071), NIA (R01
1031 AG013622), NINDS (RO1 NS106969) and from the Dr. Miriam and Sheldon G. Adelson Medical
1032 Research Foundation to A.J.S.

1033
1034 **Author contribution** YS and MZ did experimental design, data acquisition and analyses, drafting
1035 and revising the article; DC did memory linking time course and memory linking in aged *Ccr5*
1036 KO mice; GF did electrophysiology; YC and YS did qPCR; NK and WDH made the Opto-CCR5
1037 construct; JL and WDH made the Tre-mCherry construct; MK produced lentivirus with Opto-
1038 CCR5 construct. AS did memory linking in *Ccl5* KO mice; DN, CZ, AL, XK, SL, SS, MT and
1039 TS helped with data acquisition; DAF, AL and SH helped data analyses and interpretation; AJS
1040 did experimental design and interpretation, drafting and revising the article.

1041
1042 **Competing interests** The authors declare no competing interests.

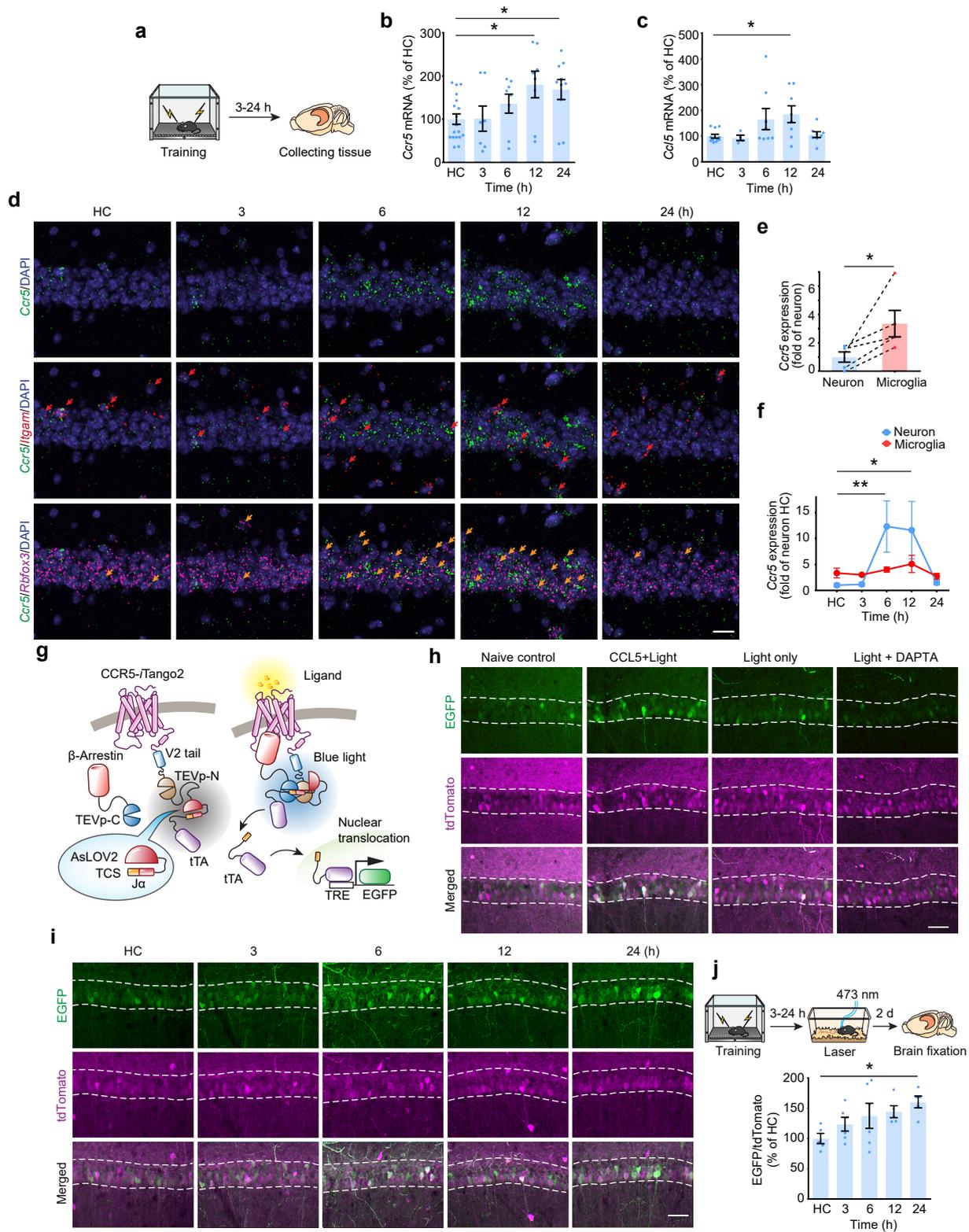
Fig. 1

Fig. 2

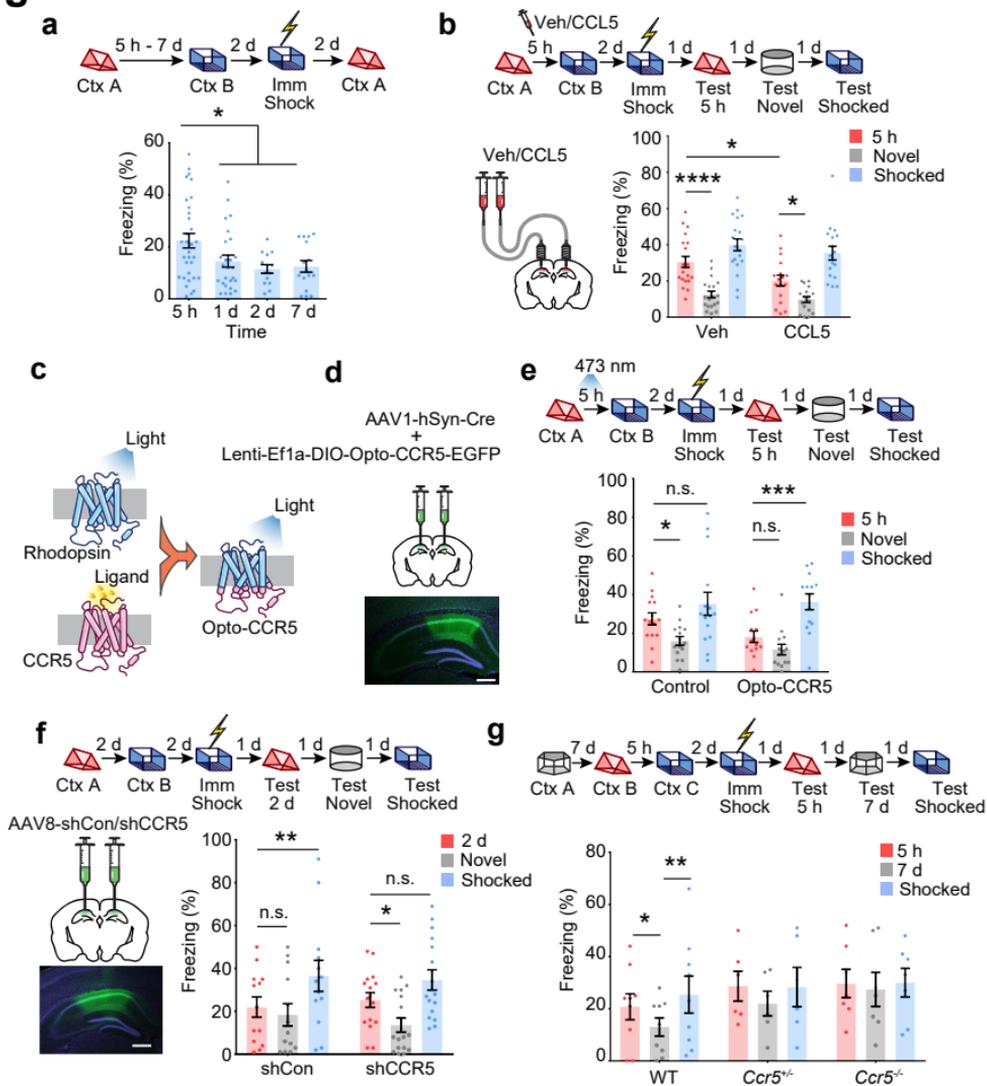


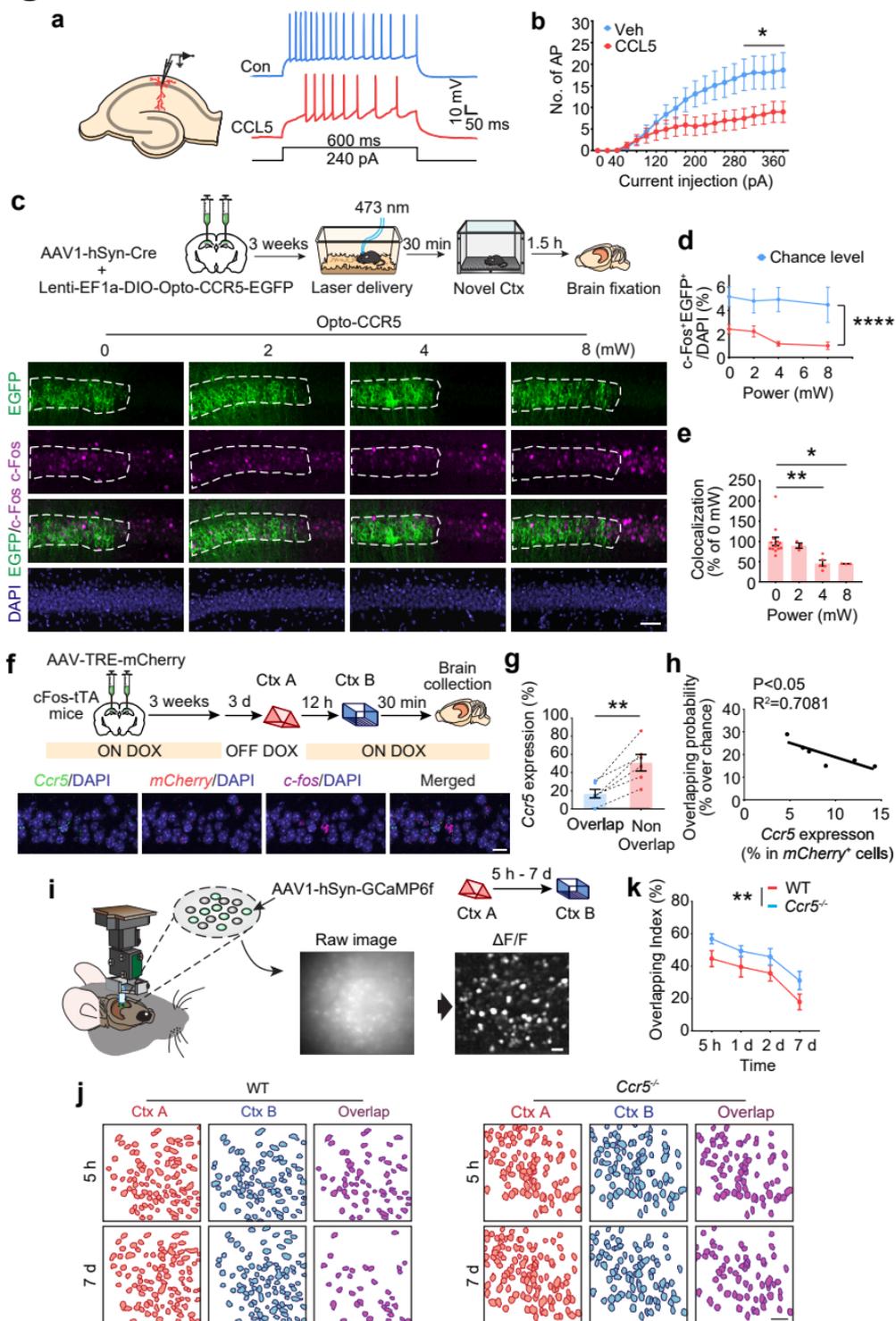
Fig. 3

Fig. 4